Induced polarization imparts piezoelectricity in noncrystalline polymer films

Xiaodong Yan,[1,2,†] Xuemu Li,[1,†] Zhihe Long,[1] Zehua Peng,[1] Jing Fu,[3] Zhuomin Zhang,[1,2]
Shiyuan Liu,[1] Ying Hong,[1] Qi Li,[3] Shujun Zhang,[4] Dragan Damjanovic,[5] and Zhengbao Yang[1,*]

[1]*Department of Mechanical and Aerospace Engineering, Hong Kong University of Science and Technology,
Clear Water Bay, Hong Kong, China*

[2]*Department of Mechanical Engineering, City University of Hong Kong, Hong Kong, China*

[3]*Department of Electrical Engineering, State Key Laboratory of Power System, Tsinghua University,
Beijing 100084, China*

[4]*Institute for Superconducting and Electronic Materials, Australian Institute for Innovative Materials, University
of Wollongong, North Wollongong, New South Wales 2500, Australia*

[5]*Institute of Materials, Swiss Federal Institute of Technology-EPFL, Lausanne 1015, Switzerland*

Piezoelectric materials produce a linear deformation in response to an applied electric field and are essential for precision-control devices. The conventional view is that polymers must be crystalline and possess remanent polarization after artificial poling to gain piezoelectricity. For the ferroelectric polymer poly(vinylidene difluoride), the required poling field is exceptionally high, up to 150–200 kV mm^{-1}. Here, we circumvent this limitation by utilizing the elastic displacement of electric dipoles and creating a net polarization. We find that a subcoercive field of 49 kV mm^{-1} can induce a high piezoelectric coefficient, d_{33}, of -33 pm V^{-1} in an unpoled poly(vinylidene fluoride-trifluoroethylene) film. In this case, the dielectric acts as a piezoelectric, as long as a bias electric field is applied, with its piezoelectric coefficient increasing proportionally to the strength of the electric field until polarization saturation sets in. The proposed methodology is further extended to amorphous polymers, providing an opportunity to discover alternative piezoelectrics within the dielectric family.

I. INTRODUCTION

Piezoelectric materials, which convert mechanical energy into electrical energy and vice versa, have been widely used in sensors, actuators, and ultrasonic transducers [1,2]. The piezoelectric materials can be classified into two main categories. One category consists of nonpolar oxides, such as quartz, where, under external stress or electric field, the dipole moment or polarization can be created because of the absence of a symmetry center [3]. The second category is polar oxides, including perovskite ferroelectrics, which possess spontaneous dipole moments. The latter have found wider applications due to spontaneous polarization and excellent piezoelectricity. However, in the original unpoled state, ferroelectric materials do not necessarily exhibit piezoelectricity because the ferroelectrics have at least two equivalent polarization vectors [4,5], where the neighboring unit cells form domains with aligned polarization. Since the domains can ideally be randomly oriented, overall, the polarization vectors of

domains cancel each other out, and the ferroelectric shows a small or even zero piezoelectric response.

The method of endowing these ferroelectrics with piezoelectricity is through artificial poling, thereby the domains are aligned along the direction of the electric field [3], and the remanent polarization is built. The critical electric field that forces domain switching is called the coercive field (E_c). For Pb(Zr, Ti)O$_3$ (PZT) based perovskite ceramics, the most extensively studied ferroelectrics in last 70 years, $E_c = 1$–3 kV mm^{-1} [6]. However, for the ferroelectric polymer poly(vinylidene difluoride) (PVDF) [7–10] and piezoelectric biopolymers such as amino acids [11–13], E_c is 1–2 orders of magnitude higher, which increases the risk of breakdown and the difficulty of artificial poling.

Another crucial challenge for ferroelectric polymers is their semicrystalline morphology [7,8,14]. This is because only crystalline regions possess long-range polar order, which can be exploited to obtain remanent polarization. However, the crystalline regions are surrounded by a considerable portion of an amorphous matrix [8]. Amorphous solids, unlike crystals, lack long-range order and their positive and negative charge centers coincide,

*Contact author: zbyang@ust.hk

[†]X. Yan and X. Li contributed equally to this work.

therefore rendering them incapable of exhibiting remanent polarization. Previous reports pointed out that the symmetry could be broken to generate induced piezoelectricity in centrosymmetric crystals and even amorphous materials by applying a dc bias electric field [15–18]; however, there is a lack of in-depth discussions, so the underlying mechanism remains obscure. It is well known that the polarization of dielectrics mainly arises from four parts, electronic polarization, ionic polarization, dipole-orientation polarization, and interfacial polarization [19], as shown in Fig. 1(a). Among them, ionic polarization exists predominantly in ionic solids, while interfacial polarization is restricted to low frequencies (<1 Hz) in semicrystalline polymers or their composites. The orientation polarization of spontaneous dipoles is limited by the crystallographic structure, and electronic polarization is present in all dielectric materials over a broad frequency range (see Appendix A). It has been recognized that the dipole moment at the molecular or lattice level can result in remanent polarization. This leads to the question of whether atomic scale polarization can be exploited to obtain polarization, and thus, piezoelectricity in dielectrics, the structures of which normally preclude piezoelectricity.

Here, we demonstrate a paradigm shift for achieving induced piezoelectricity in polymer films without permanent poling. We show that for films of the unpoled ferroelectric polymer poly(vinylidene fluoride-trifluoroethylene) [P(VDF-TrFE)] [10], a net polarization can be created by a dc bias electric field, resulting in asymmetric microstructures, and thereby, inducing linear strain under the alternating field. This occurs even at a dc bias field as low as 49 kV mm^{-1}, and the resulting piezoelectric coefficient reaches -33 pm V^{-1}, comparable to that in commercially poled P(VDF-TrFE) [9]. We emphasize that piezoelectricity induced by the subcoercive field originates from electrostriction, and its value is closely related to electronic polarization and reversible dipole-orientation polarization.

II. RESULTS AND DISCUSSION

A. Induced piezoelectricity in unpoled ferroelectric P(VDF-TrFE) polymer film

Owing to the high pliability, light weight, and low cost, PVDF and its copolymers have been widely used in electronic devices such as flexible sensors and energy harvesters [10,20]. P(VDF-TrFE), the most actively studied binary copolymer, has a coercive field as high as 60–80 kV mm^{-1} [7,8]. To achieve persistent and stable piezoelectricity, the poling electric field must be at least 150–200 kV mm^{-1}, which is 2–3 times the coercive field, making it a considerable challenge for mass production. Here, we find a solution to this challenge by utilizing a smaller bias electric field during application, which

eliminates the need for an ultrahigh poling field. This approach requires minimal additional power because polymers exhibit very low conductivity.

We prepared a ferroelectric copolymer 70/30 mol% P(VDF-TrFE) thin film by an electrohydrodynamic deposition process (Fig. S1 within the Supplemental Material [21]). The thickness of the obtained P(VDF-TrFE) film is 6.8–8.0 μm (Fig. S2 within the Supplemental Material [21]). The morphological phase transition is investigated by differential scanning calorimetry (DSC), and the crystallinity is estimated to be about 53% by integrating the melting peak (see Fig. S3 within the Supplemental Material [21] and Appendix B) [14]. The XRD results show that the crystalline region is dominated by the polar β phase (Fig. S4 within the Supplemental Material [21]) [22], which results in strong piezoelectricity of poled PVDF-based polymers [14,22].

Figure 1(b) shows the polarization-electric field hysteresis loops of the sample under different electric fields. When the electric field is less than 30 kV mm^{-1}, the maximum polarization is small (<1 μC cm^{-2}), and the polarization demonstrates a linear correlation with the electric field (Fig. S5 within the Supplemental Material [21]). As the electric field approaches 80 kV mm^{-1}, polarization undergoes a nonlinear increase (Fig. S5 within the Supplemental Material [21]). Correspondingly, domain switching occurs, which can be seen from the obvious current peak in the current-electric field curves (Fig. S6 within the Supplemental Material [21]).

In the semicrystalline ferroelectric polymer P(VDF-TrFE), polarization contributions originate from electronic polarization, dipole-orientation polarization, and interfacial polarization [Fig. 1(a) and Appendix A]. Interfacial polarization can be ignored under the current measurement frequency due to its long response time (>1 s). As shown in Fig. 1(c), the frequency-dependent relative dielectric permittivity exhibits an obvious inflection point around 1 Hz, and permittivity decreases significantly as the frequency increases, which is also consistent with the results from the frequency-dependent polarization curves at low electric field (Fig. S7 within the Supplemental Material [21]). Upon further increasing the frequency, the relative permittivity remains stable until the frequency is above 10^4 Hz. In contrast, electronic polarization occurs in an extremely short time ($<10^{-10}$ s) and the displacements are almost perfectly elastic [19], making it one of the contributors to the observed linear polarization.

The source of nonlinear polarization observed in ferroelectrics is attributed to the reorientation of spontaneous dipoles [23], which depends on the magnitude and frequency of the electric field, as shown in Fig. 1(d) and Fig. S8 within the Supplemental Material [21] (see also Ref. [24]). It can be seen that polarization increases with decreasing frequency. When the frequency is down to 0.1 Hz, or even 0.01 Hz, leakage occurs [25]. At such low
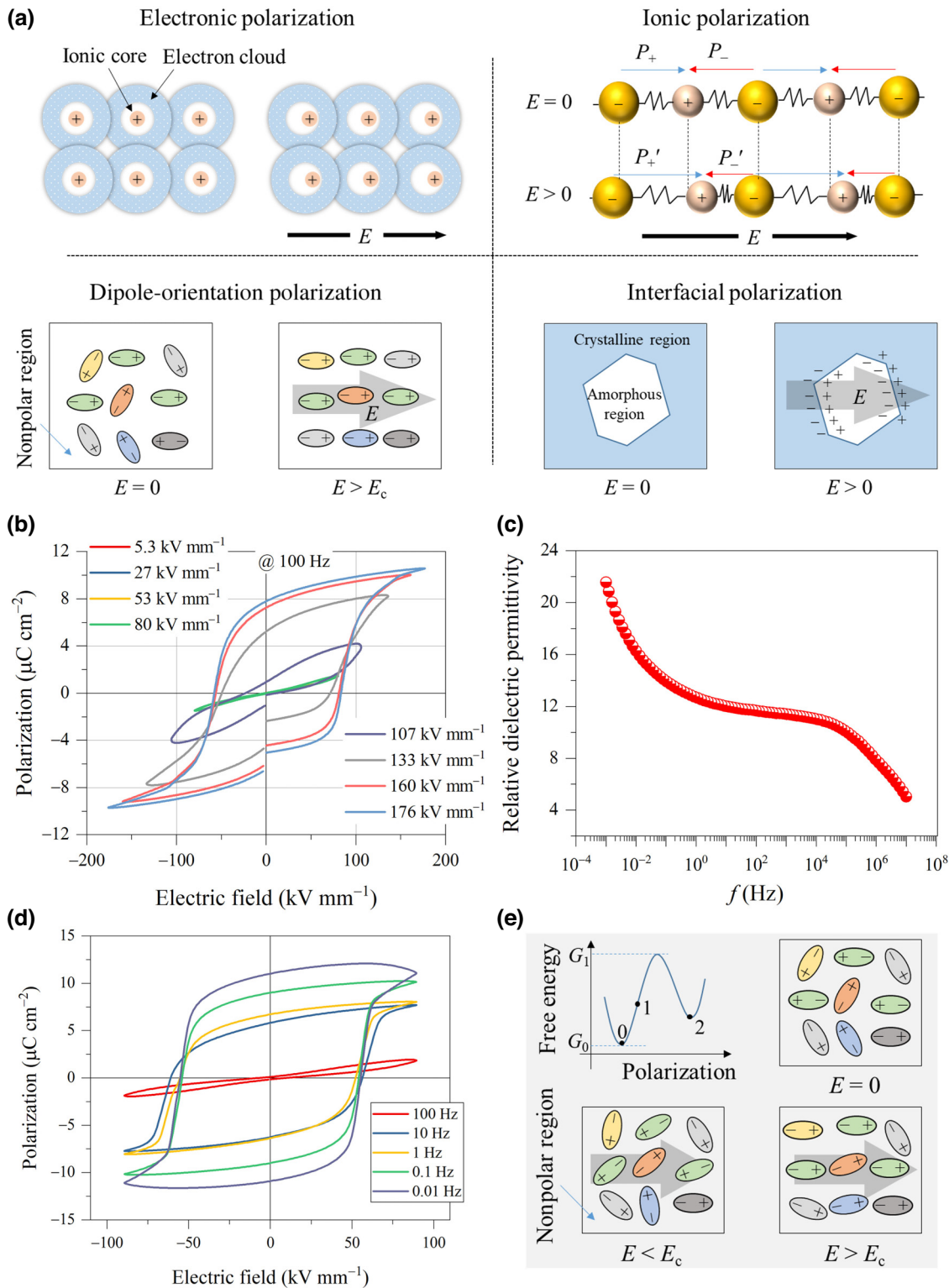
FIG. 1. Polarization mechanisms and polarization behavior of P(VDF-TrFE) films. (a) Schematic representation of the four polarization mechanisms of dielectrics. (b) Polarization-electric field hysteresis loops under electric fields from 5.3 to 176 kV mm^{-1}; measurement frequency is 100 Hz. (c) Frequency-dependent relative dielectric permittivity measured under a voltage of 1 V. (d) Polarization-electric field loops under various measuring frequencies. (e) Schematic diagram of the free-energy profile for a system with polarization, and the orientation of dipoles at three stages under different electric fields. Numbers represent the energy states of the three stages of polarization switching, colors of the dipoles distinguish their initial orientations, and translucent gray arrows indicate the direction of the electric field.

frequencies, part of the observed polarization comes from interfacial polarization.

From a thermodynamic point of view [23,26], in the initial state, the spontaneous dipoles are locate at a stable state with the free-energy (G) minimum, which is designated as position "0" on the energy profile [Fig. 1(e)]. For P(VDF-TrFE) with a hexagonal crystal structure [20,22], the angles between the dipole vectors are 60°, 120°, and 180°. When a small electric field is applied, the dipole orientations change slightly, which will also contribute to linear polarization. Meanwhile, the system energy slightly increases to position "1," but the energy supplied to the system is insufficient to overcome the energy barrier ($\Delta G = G_1 - G_0$) required for dipole flipping; as a result, the dipole is trapped in a metastable state and will return to its initial orientation once the electric field is removed. When the energy applied to the system surpasses ΔG, the spontaneous dipoles completely flip and align along the direction of the electric field. When the electric field is withdrawn, a new energetically stable state is reestablished (position "2"). Thus, the net polarization significantly increases due to the alignment of the dipoles; the process is irreversible and is a major contributor to the nonlinear polarization of ferroelectric materials. It should be noted that the poling field is usually required to be at least twice that of the coercive field to achieve a stable and permanently polarized state.

In this context, when the electric field is below E_c, induced polarization occurs in P(VDF-TrFE) [7], which is characterized by linear polarization behavior attributed to electronic displacement and reversible dipole-orientation polarization. The slope of the polarization-electric field curve is proportional to the relative dielectric permittivity, and the obtained value is about 9.7, which is consistent with the result measured under a small signal voltage of 1 V [Figs. 1(c) and S9 within the Supplemental Material [21]]. Under an electric field greatly surpassing E_c, e.g., 160 kV mm^{-1} [Fig. 1(b)], polarization increases substantially and the hysteresis loop is almost saturated. We can observe that the remanent polarization is about 6.8 μC cm^{-2} and E_c is about 71 kV mm^{-1} at a frequency of 100 Hz. The total polarization will consist of both the induced polarization (P_i) and the spontaneous polarization (P_s) [7], as follows:

$$P = P_i + P_s = \varepsilon E + P_s, \tag{1}$$

where ε is the dielectric permittivity.

A ferroelectric without artificial poling does not exhibit piezoelectricity due to the absence of remanent polarization; however, it will be electrostrictive under an electric field because of the anharmonic shifts of atoms or ions in all dielectrics [27]. We measured the electromechanical response of P(VDF-TrFE) films under an ac electric field (E_{ac}). The displacement of the film along the

thickness direction was measured by a contactless laser method, as shown in Fig. 2(a). Figure 2(b) shows the input voltage and output displacement waveforms; the amplitude of the applied electric field is about 27 kV mm^{-1}, which is much lower than E_c of the P(VDF-TrFE) film. We can observe a clear displacement response and find that the period of the displacement waveform is half that of the input voltage waveform. For the input harmonic signal, it can be expressed as $U = U_0 \sin 2\pi ft$, where U_0 is the amplitude of the input ac voltage, f is the frequency, and t is the response time. The strain from the electrostrictive effect is expressed as $S_e = ME^2$, where M is the electrostrictive coefficient [28–30], since $(\sin 2\pi ft)^2 = 1/2[1 - \cos 4\pi ft]$, we observed the second-harmonic displacement response. Unlike PZT, the sign of the P(VDF-TrFE) film's electrostrictive coefficient is negative (Fig. S10 within the Supplemental Material [21] and Appendix C). Figure 2(c) shows the corresponding FFT amplitude spectra of the generated displacement signal. When the frequency of the input voltage signal is 500 Hz, the displacement signal reaches its peak at 1000 Hz. In addition, we fit the strain data with different ac field amplitudes and find that they follow the parabolic law [Fig. 2(d)]. The obtained electrostrictive coefficient (M_{33}) is about -3.6×10^{-19} m^2 V^{-2}, which is comparable to the previously reported values (calculated M_{33} is -3.8–4.4×10^{-19} m^2 V^{-2}) [7–9].

Although the switching of spontaneous dipoles does not occur at low electric fields, we can exploit induced polarization. The inversion symmetry of bound charges in the dielectrics can be broken by applying a dc bias field [20,28,31,32], leading to asymmetric charge distribution and induced polarization. Under the concurrent application of a dc electric field ($E_{dc} \sim 68$ kV mm^{-1}) and an ac electric field ($E_{ac} \sim 27$ kV mm^{-1}), we observe a first-harmonic displacement that corresponds to the frequency of the electric field at 500 Hz, as shown in Fig. 3(a). The deformation of the polymer sample under an ac + dc electric field can be attributed to two aspects. First, it is thermal expansion due to the Joule heating effect. However, the PVDF-based polymer has a positive thermal-expansion coefficient [33] while we observe a negative strain, eliminating this explanation. Alternatively, the deformation can be caused by the electromechanical coupling effect. As shown in Fig. S11 within the Supplemental Material [21], we observe that, when the dc bias field is positive, the phase of the output displacement is opposite to that of the input ac voltage. This indicates that the sample contracts when the direction of the ac field aligns with the induced-polarization direction (see Appendix D). We thus can conclude that the generated deformation in the P(VDF-TrFE) film is primarily due to the negative piezoelectric effect [7,9]. More importantly, the generated displacement does not attenuate significantly under the continuous dc bias field (Fig. S12 within the Supplemental Material [21]).
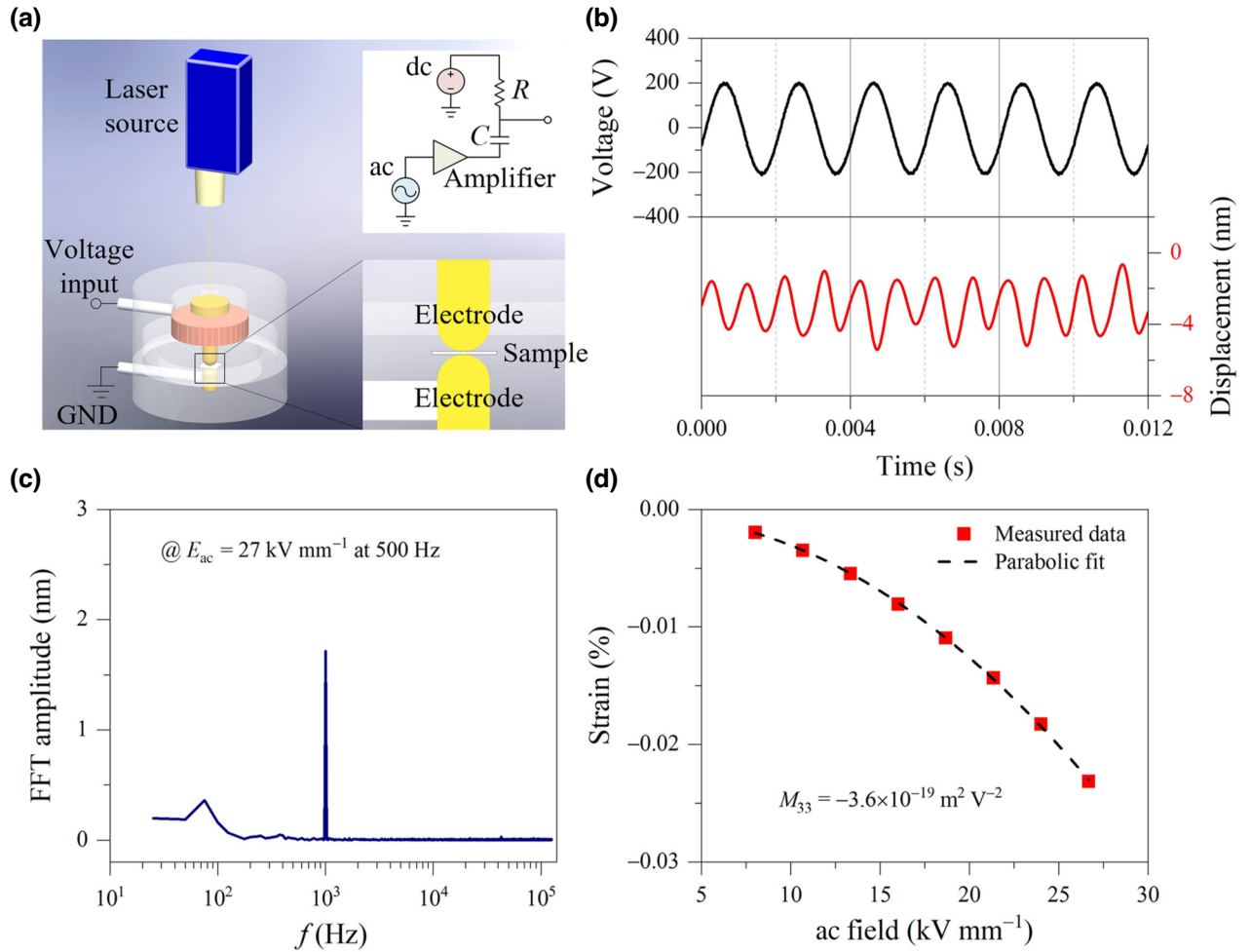
FIG. 2. Electric-field-induced electrostrictive response of P(VDF-TrFE) films. (a) Schematic diagram of the experimental setup, simultaneously recording the input voltage and the output displacement. Dimensions of the sample are 15×15 mm^2 and 7.5 μm thick. Upper-right corner shows the equivalent circuit of the voltage source. (b) Time-resolved harmonic displacement response under an electrical input of $E_{ac} = 27$ kV mm^{-1} at $f = 500$ Hz. (c) Corresponding fast Fourier transform (FFT) amplitude spectra of the generated harmonic displacement as a function of frequency. (d) Electrostrictive strain as a function of E_{ac} measured at 500 Hz. Dashed line represents the parabolic fit.

Figure 3(b) is the fast Fourier transform amplitude spectra corresponding to the displacement signal. In addition to the first-harmonic displacement, a weak second-harmonic displacement response can also be observed at 1000 Hz because E_{ac} is much smaller than that of E_{dc}. Once the magnitude of E_{ac} is comparable to or even higher than E_{dc}, we can observe an asymmetric response consisting of the first and second harmonics (Fig. S13 within the Supplemental Material [21]).

We measured the variation of the piezoelectric strain with the amplitude of the ac field under different dc bias fields, as shown in Fig. 3(c). For a specific dc bias field, piezoelectric strain increases linearly with the ac amplitude, following the piezoelectric strain equation: $S_p = dE_{ac}$. Under a dc bias field of 68 kV mm^{-1} and an ac field of 27 kV mm^{-1}, the piezoelectric strain is as high as −0.1%, corresponding to an effective piezoelectric strain

coefficient of −36 pm V^{-1}. It should be noted that the piezoelectric coefficient varies as a function of the dc bias field, where the piezoelectric coefficients are −27, −33, and −36 pm V^{-1} at dc bias fields of about 37, 49, and 68 kV mm^{-1}, respectively.

Under the measuring electric field, P(VDF-TrFE) shows linear polarization behavior [7], as $P = \varepsilon E$. According to the phenomenological theory [34,35], the piezoelectric coefficient, d, is closely related to the electrostrictive coefficient, permittivity, and polarization, by

$$d = 2QP\varepsilon, \qquad (2)$$

where Q is the polarization-related electrostrictive coefficient; the formula $M = Q\varepsilon^2$ holds for linear dielectrics [27]. Thus, the induced piezoelectric coefficient, d_{ind},

(a)

(b)

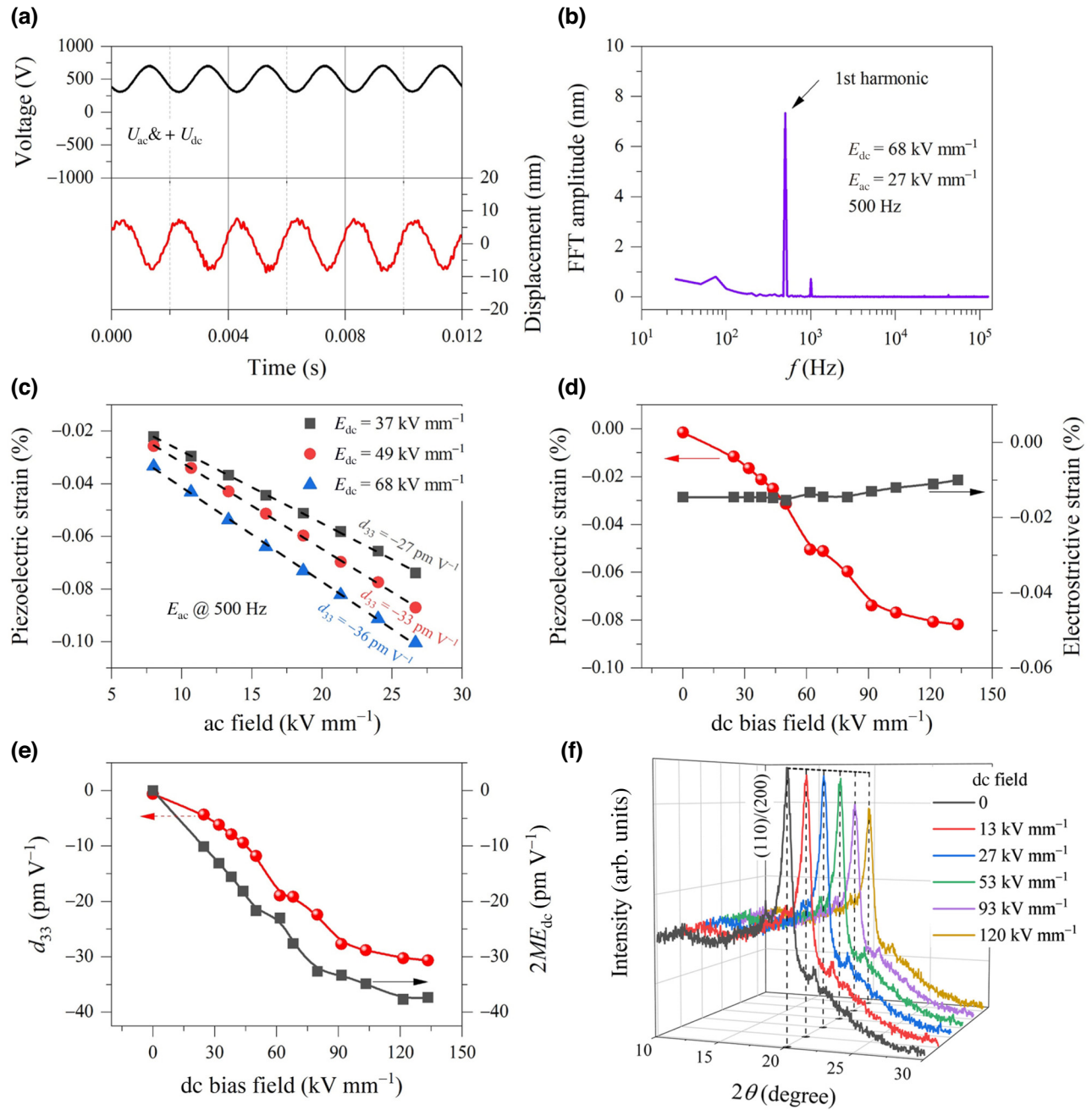
(c)

(d)

(e)

(f)

FIG. 3.　Induced piezoelectric displacements in P(VDF-TrFE) films. (a) Time-resolved harmonic electromechanical displacements measured at 500 Hz and excited by $E_{ac} = 27$ kV mm^{-1} under $E_{dc} = 68$ kV mm^{-1}, where the offset of the displacement signal is discarded before the curve is plotted. (b) FFT amplitude spectra of the first-harmonic displacement generated as a function of frequency. (c) Linear piezoelectric strain as a function of E_{ac} with $E_{dc} \sim 37$, 49, and 68 kV mm^{-1} measured at 500 Hz. Dashed line represents the linear fit. (d) Concurrently measured first- and second-harmonic displacements under constant $E_{ac} = 27$ kV mm^{-1} and various E_{dc}. (e) Induced d_{33} and $2ME_{dc}$ with various E_{dc} under constant E_{ac}. (f) XRD 2θ patterns of the film under various *in situ* E_{dc} applications. Dashed line represents reference values.

under the bias electric field can be derived as

$$d_{\text{ind}} = 2ME_{\text{dc}}. \quad (3)$$

The formula shows that d_{ind} is related to M and the bias electric field. To verify this, we measured the displacement

of the P(VDF-TrFE) film under a constant ac field and various dc bias fields. We set the ac field to be 27 kV mm^{-1} and the maximum dc bias field to be 133 kV mm^{-1}, so both the first- and second-harmonic displacements can be detected. We find that the absolute value of the piezoelectric strain first increases rapidly with the dc bias field, until it

approaches a value of about $90 \, \text{kV} \, \text{mm}^{-1}$, above which the strain continues to increase but at a slower pace, as shown in Fig. 3(d). On the other hand, the absolute value of electrostrictive strain remains almost constant with E_{dc} below $90 \, \text{kV} \, \text{mm}^{-1}$, and then decreases slightly. We obtained d_{33} and M_{33} using the piezoelectric and electrostrictive strains, and calculated the $2ME_{\text{dc}}$ value, as shown in Fig. 3(e). The results indicate a clear correlation between the variation of $2ME_{\text{dc}}$ and d_{33}, with both exhibiting almost identical patterns, even if the former value is slightly higher than the latter one.

It was reported that the origin of the piezoelectricity for poled PVDF-based polymers was electrostriction [7,9]. The application of a low dc bias field does not substantially impact the dimensions of the crystalline region and the crystal structure of P(VDF-TrFE) [20,36]. As shown in Fig. 3(f), when the applied dc bias field is lower than $53 \, \text{kV} \, \text{mm}^{-1}$, there is minimal variation in the peak position and intensity of the (110)/(200) diffraction of the β phase. When the P(VDF-TrFE) film is subjected to a sub-coercive field, the induced polarization increases linearly with the strength of the electric field, that is, the linear change in the electric dipole moment leads to an induced d_{33} that is almost proportional to the dc bias field. When the applied dc bias field is higher than $93 \, \text{kV} \, \text{mm}^{-1}$, the intensity of the (110)/(200) diffraction is significantly reduced, implying a decrease in the coherent crystallization region [20]. The calculated results (see Appendix E) show that the crystallite size decreases from 15.2 nm ($53 \, \text{kV} \, \text{mm}^{-1}$) to 13.0 nm ($93 \, \text{kV} \, \text{mm}^{-1}$). Previous reports pointed out that the ordered structure with a small rattling space generally exhibited a larger Q [27]. Therefore, decreased M_{33} under E_{dc} above $90 \, \text{kV} \, \text{mm}^{-1}$ can be linked to the suppression of Q by the reduction of the microcrystalline size.

B. Induced piezoelectricity in noncrystalline dielectric polymers and biological materials

The above results indicate that the induced piezoelectricity in the ferroelectric films studied are closely related to the electrostrictive coefficient, M, in the subcoercive field. Since domain switching does not contribute to this process, the induced-piezoelectricity method should not be limited solely to ferroelectric polymers, but rather, it should be applicable to all dielectrics, including noncrystalline ones [32].

We next apply the same approach to induce a piezoelectric effect in nonferroelectric polymers. We prepared two kinds of polymer films, polyvinyl alcohol (PVA) and a biological tissue. PVA is a nontoxic, biocompatible, and linear synthetic polymer [37]. Due to good adhesion and plasticity, it is widely used as a plasticizer for forming inorganic powders and as a matrix for flexible piezoelectric composites, but it does not show piezoelectricity itself. We prepared PVA films (Fig. S14 within the Supplemental

Material [21]) by an electrohydrodynamic deposition process (Fig. S1 within the Supplemental Material [21]). The broad reflection peak of the XRD pattern at $2\theta \sim 20°$ (Fig. S15 within the Supplemental Material [21]) indicates a semicrystalline morphology [38]. The DSC analysis (Fig. S16 within the Supplemental Material [21], see also Refs. [39–41]) shows that its crystallinity is about 12%. Although the arrangement of atoms or molecules exhibits a certain level of localized order on a small length scale, it does not possess long-range order and has a structure that is similar to that of amorphous materials [42,43]. Figure S17 within the Supplemental Material [21] shows its polarization-electric field curves; no hysteresis is observed, even under electric fields as high as $226 \, \text{kV} \, \text{mm}^{-1}$, and remanent polarization is always less than $1 \, \mu\text{C} \, \text{cm}^{-2}$, thus ruling out the possibility of permanent poling.

We measured the electromechanical response of the PVA film under an ac electric field (Fig. S18 within the Supplemental Material [21]), the results show that the electrostrictive coefficient (M_{33}) is about $-1.9 \times 10^{-19} \, \text{m}^2 \, \text{V}^{-2}$. Induced displacement under an ac + dc electric field was also observed [Fig. 4(a)]; the phase relationship of the voltage and displacement waveforms implies the negative piezoelectric effect in PVA, which is attributed to the dimensional effect caused by van der Waals forces [7,9,44]. Under a dc bias field of about $48 \, \text{kV} \, \text{mm}^{-1}$, we observe that the first-harmonic strain increases linearly with increasing ac field, as shown in Fig. 4(b). As a result, the piezoelectric coefficient is $-25 \, \text{pm} \, \text{V}^{-1}$.

Piezoelectric biomaterials, such as piezoelectric biological tissues, have attracted extensive attention in recent years due to their advantages of biocompatibility, absorbability, and degradability. However, due to the large molecular polarity and complex assembly, biopolymers are difficult to permanently pole and show minimal piezoelectricity on the macroscopic level [11,45]. It was reported that small intestinal submucosa (SIS) was a semicrystalline organic biomaterial, mainly composed of amorphous collagen fibers [46]. We prepared SIS films (Figs. S19 and S20 within the Supplemental Material [21]) through an exfoliation process [47]. The polarization measurements show that it is not ferroelectric under the current electric field (Fig. S21 within the Supplemental Material [21]), and due to the loose microstructure (Fig. S19 within the Supplemental Material [21]), the breakdown strength is very low, and the maximum polarization is even less than $0.1 \, \mu\text{C} \, \text{cm}^{-2}$. Nevertheless, we can also observe clear displacement responses under ac (Fig. S22 within the Supplemental Material [21]) and ac + dc (Fig. S23 within the Supplemental Material [21]) electric fields. Under a dc bias field of about $40 \, \text{kV} \, \text{mm}^{-1}$, the piezoelectric coefficient is $-13 \, \text{pm} \, \text{V}^{-1}$.

Our results demonstrate that electrostrictive materials can be operated in the field-biased piezoelectric mode,
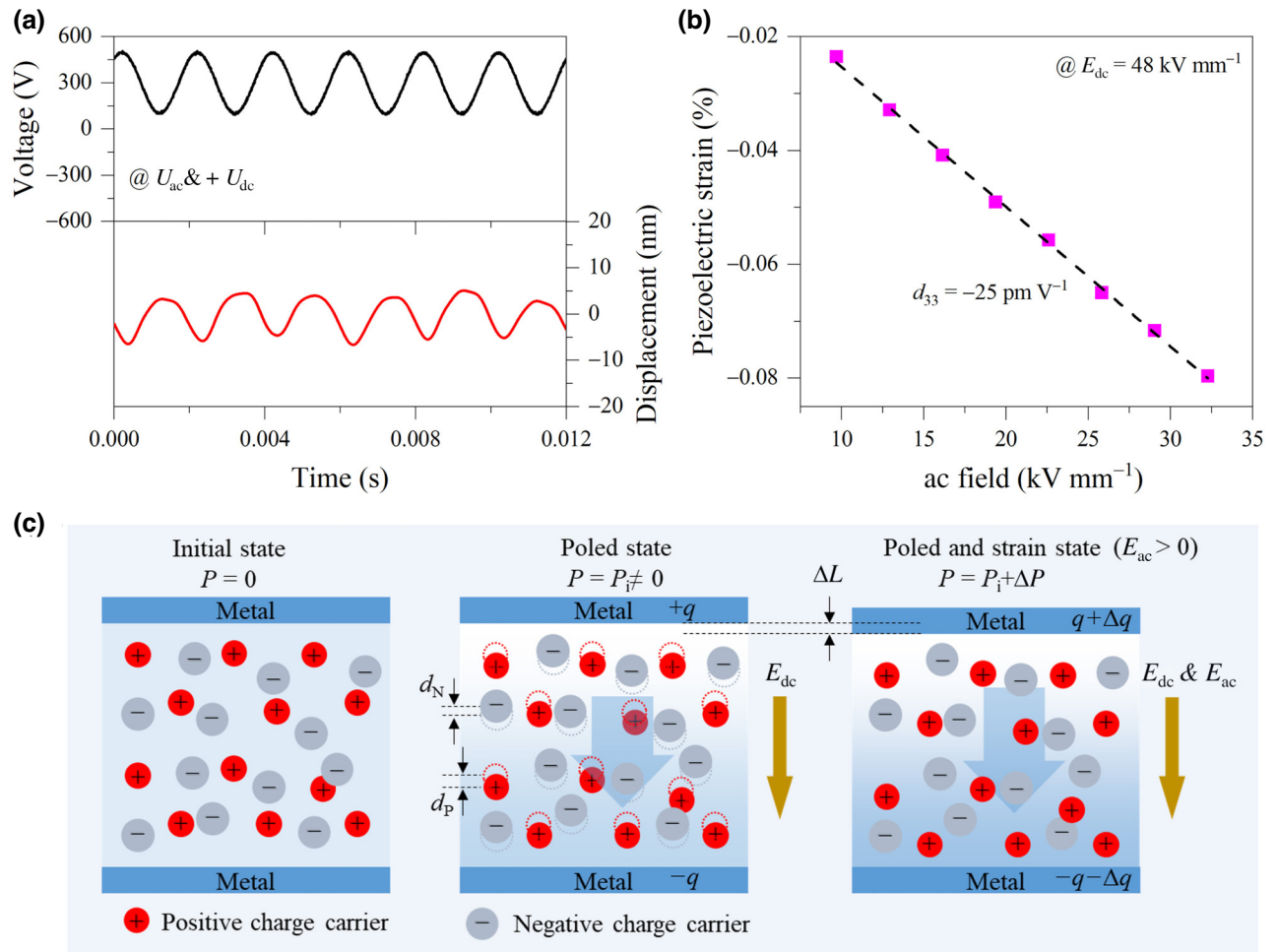
FIG. 4. Induced piezoelectricity and the proposed mechanism in dielectric films with linear polarization. (a) Time-resolved harmonic electromechanical displacement of polyvinyl alcohol film under an ac + dc field. (b) Piezoelectric strain of the film varies with the ac field amplitude at $E_{dc} = 48$ kV mm^{-1}. Dashed line represents the linear fit. (c) Schematic diagram of induced piezoelectric strain under an ac + dc field. Dotted circle represents the initial position of the charge carrier; d_P and d_N represent the displacement of positive and negative charge carriers, respectively; and ΔL represents the macroscopic deformation of the sample. Under a dc bias field, charge carriers with opposite signs move relative to each other, and the dielectric has an induced polarization. Simultaneously applying ac and dc fields, the small electric field disturbance causes a change in the amount of induced charge on the electrode surface. Here, $E_{ac} > 0$ means that the direction of E_{ac} is consistent with that of E_{dc}. Thus, the amount of induced charge increases, and the sample contracts due to the dimensional effect [9] of the polymer.

whether they are crystalline, noncentrosymmetric, or polar [3,32]. In the present case, a dc bias field is applied to the film to induce polarization, whereupon the material acts as a piezoelectric as long as the field is applied [Fig. 4(c)]. When ac and dc fields are simultaneously applied, the ac field's small disturbance causes a change in the amount of charge on the electrode surface, which, in turn, leads to a linear deformation of the film. Specifically, when $E_{ac} > 0$, the surface charge increases, and the polarization of dielectrics must increase accordingly to accommodate the change. In polymers, the intermolecular van der Waals force is much weaker than the covalent bond in the molecule. Under the application of a small ac field, the interaction between molecules is more easily

affected. As a result, the molecular distance of the polymer will decrease and the sample will contract, so that the dipole moment per unit volume increases, i.e., the dimensional effect [9]. Moreover, the stronger the dc bias field, the larger the strain and piezoelectric effect until polarization saturation sets in. In practical applications, applying a bias electric field is easy to implement, especially for actuators, where the bias of an ac signal can be achieved simply by designing the capacitance and resistance of the circuit. More importantly, this method will greatly broaden the types of dielectric materials for actuators and may even solve the hysteresis and temperature stability issues of piezoelectric strain in traditional oxide ferroelectric materials.

III. CONCLUSION

We demonstrate the possibility of achieving large piezo-electricity by electric-field-induced symmetry breaking in dielectric polymers. Our results show that a piezoelectric coefficient of -33 pm V^{-1} can be induced in unpoled P(VDF-TrFE) polymer films by applying a dc bias field of <50 kV mm^{-1}. By exploiting atomic scale electric dipoles, net polarization is built in ferroelectric films even, under a subcoercive field, thus a linear electromechanical response is induced under the concurrent application of ac and dc fields. This strategy can even be extended to amorphous dielectric films. Our findings provide a good paradigm to revamp piezoelectricity in polymers by exploiting the electrostriction of materials, thus presenting an alternative design strategy for a wide range of eco-friendly functional materials.

IV. MATERIALS AND METHODS

A. Preparation of inks

Inks of P(VDF-TrFE) copolymer are prepared by dissolving 1-g P(VDF-TrFE) powder (VDF/TrFE $=$ 70/30 mol, Piezo Technologies, France) in 10-ml N,N-dimethylformamide (Sigma-Aldrich), and stirring at 70 °C for 12 h to form homogeneous solutions.

Inks of PVA are prepared by dissolving 5-g PVA particles (with average molecular weight 57 000–66 000 g mol^{-1} and 98–99% hydrolyzed, Alfa Aesar) in 100-ml distilled water at 70 °C for 3 h. Once PVA is completely dissolved, it is stirred overnight at room temperature to form homogeneous solutions.

Inks of PZT are prepared by the following steps. First, the Pb$_{1.2}$(Zr$_{0.52}$Ti$_{0.48}$)O$_3$ sol was prepared. Lead(II) acetate trihydrate, [Pb(CH$_3$COO)$_2$] · 3H$_2$O (99%, TCI), is first dissolved in acetic acid (99%, TCI) at 120 °C and mixed by magnetic stirring. When it is completely dissolved, the solution is cooled to room temperature. Zirconium(IV) n-propoxide (C$_{12}$H$_{28}$O$_4$Zr, 70 wt% in 1-propanol, TCI) is mixed with titanium(IV) butoxide (C$_{16}$H$_{36}$O$_4$Ti, 99%, TCI) in another container. Then, zirconium(IV) n-propoxide and titanium(IV) butoxide are added to lead(II) acetate solution, and diluted with ethylene glycol (99.5%, Dieckmann) to 0.2 mol L^{-1} with stirring for 6 h in air. Finally, inks of PZT slurry are prepared by adding the proper amount of commercial PZT powders (typically 30–50 wt%, particle size of <500 nm) to the PZT sol and homogenizing the mixture by ball milling.

B. Deposition of thin films

The films are prepared by electrohydrodynamic deposition (Fig. S1 within the Supplemental Material [21]). Inks are loaded into a 5-ml syringe and supplied to a metal nozzle [inner (outer) diameter of 0.6 (0.91) mm] by a syringe pump (Lead fluid apparatus, Pump TYD01) with the flow rate of 10–20 μl min^{-1}. Si (100) wafer (thickness of 500 μm, n-type) is used as a substrate and cleaned with ethanol prior to deposition. A positive potential is applied to the nozzle using a high-voltage supply (DW-P303–1ACH2, Dongwen High Voltage Power Supply Co., Ltd.), while the nozzle-to-substrate distance is kept to 8–10 mm. The substrate is positioned on an electrically grounded plate, mounted atop of an X-Y translation stage. Electrohydrodynamic jetting is formed by increasing the nozzle voltage to 3000–7000 V, until the pendant liquid drop elongates, splits into multiple micro- and nanojets, and falls onto the substrate. During deposition, the substrate is alternately rastered with the major scan in the X and Y directions with a speed of 10–30 mm s^{-1}. Deposition is carried out under ambient conditions, with a relative humidity of 50–70% and temperature of 22–26 °C. After the deposition of two layers, the wet P(VDF-TrFE) polymer films are dried at 70 °C for 5 min and annealed at 110 °C for 24 h. The wet PVA films are dried at 70 °C for 30 min. For deposited PZT precursors, sol infiltration into every five layers of the as-prepared films by means of spin-coating is performed. Sintering treatment at 800 °C for 30 min is performed to synthesize perovskite structures.

C. Structural characterization

To observe the morphology of the samples, the film was immersed in liquid nitrogen, and the cross section of the sample was obtained after bending and brittle fracture. The cross-section morphology of the sample was observed by a scanning electron microscope (Quanta 450, FEI). The heat-flow curves of the samples were obtained by using a differential scanning calorimeter (DSC3, Mettler Toledo) at a heating rate of 5 °C min^{-1}. The crystal structure of the sample was examined by using an x-ray diffractometer (D8 Advance, Bruker). For in $situ$ crystal-structure measurements, gold electrodes were prepared by using a magnetron sputter (Q150T ES Plus, Quorum Technologies); the thickness of the gold electrodes was about 10 nm, and the diameter of the circular electrodes was controlled by a mask to be 10 mm. The voltage was applied to the sample through a high-voltage dc power supply (TCM6000i, Dalian Teslaman Tech. Co., Ltd.), and x-ray diffraction was performed after the voltage was stabilized.

D. Dielectric property measurements

The capacitance and loss of the P(VDF-TrFE) film sample were measured by using an inductance-capacitance-resistance (LCR) meter (E4980A, Agilent Technologies, Inc.), and the applied voltage was 1 V. During the measurement, the sample chamber was evacuated, and the temperature was controlled by a program controller; the heating rate was 3 °C min^{-1}. The capacitance of the sample in the frequency range of 10^{-3}–10^7 Hz was measured

by using a broadband impedance spectrometer (Concept 40, Novocontrol Technologies).

E. Ferroelectric property measurements

To determine the ferroelectric properties, in the process of magnetron sputtering, the diameter of the circular electrode is 2 mm under the control of a mask, and the polarization-electric field hysteresis loop of the sample is obtained by using a ferroelectric instrument (CPE1801, PolyK Technologies, LLC) at 100 Hz. The frequency-dependent *P-E* loops and *S-E* curves were measured using a ferroelectricity analyzer (Aix ACCT, TF Analyzer 1000, Aachen, Germany).

F. Strain measurements

We measured the displacement of the sample by a contactless laser method. The electric field was applied to the film without artificial poling treatment; the type, amplitude, and frequency of the electric field were controlled by a function generator (DG1062, RIGOL Technologies Co., Ltd.), a power amplifier (E01.A2, Harbin Core Tomorrow Science and Technology Co., Ltd.), and a high-voltage dc power supply (TCM6000i, Dalian Teslaman Tech. Co., Ltd.) The displacement of the sample was captured by a laser vibrometer (NLV-2500, Polytec GmbH) with a sensor sensitivity of 50 nm V^{-1} and a resolution of 15 pm. Then, the displacement signal and the input voltage signal were simultaneously monitored by the digital storage oscilloscope (RTE 1024, Rohde & Schwarz USA, Inc.)

All data are available in the main text or within the Supplemental Material [21].

APPENDIX A: DIELECTRIC POLARIZATION MECHANISM

Four types of polarization can be induced in dielectrics [19]: electronic polarization due to the displacement of electrons with respect to positive nuclei within the atom, ionic polarization due to the displacement of charged atoms with respect to each other in certain ionic crystals, dipole polarization due to the effect of the applied field on the orientations of permanent dipole moments, and finally interfacial polarization caused by the accumulation of free ions at the interfaces between materials with different conductivities and dielectric constants.

Dielectric polarizations are classified as instantaneous polarizations and absorptive polarizations [19]. Instantaneous polarizations may be thought of as polarizations that can form completely in times less than say 10^{-10} s. Among the above polarization types, electronic polarization and ionic polarization are instantaneous polarization. Dipole polarizations can form in times from 10^{-8} to 10^{-2} s. However, the interfacial polarization takes longer to establish, >1 s.

APPENDIX B: CALCULATION OF CRYSTALLINITY

The degree of crystallinity (x_c) can be calculated using the following equation [48]:

$$x_c = \frac{\Delta H_m}{\Delta H_0},\qquad (B1)$$

where ΔH_m is the enthalpy of melting of the sample, which can be obtained by integrating the melting peak in the DSC curves, near 150 °C for P(VDF-TrFE). ΔH_0 is the enthalpy of melting of materials that are 100% crystalline; for pure P(VDF-TrFE), ΔH_0 is 40 J g^{-1}.

APPENDIX C: THE SIGN OF THE ELECTROSTRICTIVE COEFFICIENT

When the dielectric material is excited by an electric field with a sine wave, the input voltage and the generated electrostrictive strain can be expressed as [28]

$$U(t) = U_0 \sin 2\pi f t,\qquad (C1)$$

$$S_e(t) = ME^2(t) = \frac{M}{2}\frac{U_0^2}{L^2}(1 - \cos 4\pi f t),\qquad (C2)$$

where L is the sample thickness. According to the phase relationship of the harmonic function, if M is positive, we know that regardless of whether the input sine is located at the peak ($2\pi f t = \pi/2$) or the valley ($2\pi f t = 3\pi/2$), the output strain is located at the peak ($4\pi f t = n\pi$, n is odd number). Conversely, if M is negative, the output strains are all located in valley, as shown by the blue dotted line

in Fig. S10(a) within the Supplemental Material [21]. We also find that the phase difference of the displacement sines of P(VDF-TrFE) and PZT films is π (Fig. S10 within the Supplemental Material [21]), implying that their signs are opposite. These results indicate that the sign of the electrostriction coefficient of P(VDF-TrFE) is negative.

APPENDIX D: THE SIGN OF THE PIEZOELECTRIC STRAIN COEFFICIENT

There is no doubt that the direction of induced polarization must be along that of the dc bias field. Under a positive bias field, when the input ac sine is at the peak, the direction of the ac field is consistent with the polarization direction, thus its sign is positive. For P(VDF-TrFE), at this time, the displacement sine is in the valley, thus the sample shrinks relative to the initial thickness, so the strain is negative, as shown by the blue diamond symbol in Fig. S11(a) within the Supplemental Material [21]. According to the piezoelectric equation, the sign of the piezoelectric coefficient is negative. In contrast, the output displacement sine of PZT has the same phase as the input ac sine [Fig. S11(b) within the Supplemental Material [21]], which indicates that the sign of its piezoelectric coefficient is positive.

In addition, we intercepted simultaneous data of displacement and ac voltage and plotted them in Figs. S11(c) and S11(d) within the Supplemental Material [21]. As we can see, for P(VDF-TrFE) films, the slope of the curve is <0, indicating a negative piezoelectric coefficient.

APPENDIX E: CALCULATION OF P(VDF-TrFE) CRYSTALLITE SIZE

The crystallite size was calculated using Scherrer's formula [49]:

$$b = \frac{K\lambda}{L\cos\theta}, \tag{E1}$$

where b is the FWHM in radians; λ is the wavelength of the x-ray beam (1.54056 Å); L is the crystallite size in Å; and K is a constant, which varies from 0.89 to 1.39, but for most cases it is close to 1.

---

[1] G. Huangfu, K. Zeng, B. Wang, J. Wang, Z. Fu, F. Xu, S. Zhang, H. Luo, D. Viehland, and Y. Guo, Giant electric field-induced strain in lead-free piezoceramics, Science **378,** 1125 (2022).

[2] J. Rodel, W. Jo, K. T. P. Seifert, E. M. Anton, T. Granzow, and D. Damjanovic, Perspective on the development of lead-free piezoceramics, J. Am. Ceram. Soc. **92,** 1153 (2009).

[3] G. H. Haertling, Ferroelectric ceramics: History and technology, J. Am. Ceram. Soc. **82,** 797 (1999).

[4] A. D. Moriana and S. Zhang, Lead-free textured piezoceramics using tape casting: A review, J. Materiomics **4,** 277 (2018).

[5] C. R. Qiu, B. Wang, N. Zhang, S. J. Zhang, J. F. Liu, D. Walker, Y. Wang, H. Tian, T. R. Shrout, Z. Xu, L. Q. Chen, and F. Li, Transparent ferroelectric crystals with ultrahigh piezoelectricity, Nature **577,** 350 (2020).

[6] T. R. Shrout and S. J. Zhang, Lead-free piezoelectric ceramics: Alternatives for PZT?, J. Electroceram. **19,** 113 (2007).

[7] I. Katsouras, K. Asadi, M. Li, T. B. van Driel, K. S. Kjær, D. Zhao, T. Lenz, Y. Gu, P. W. M. Blom, D. Damjanovic, M. M. Nielsen, and D. M. de Leeuw, The negative piezoelectric effect of the ferroelectric polymer poly(vinylidene fluoride), Nat. Mater. **15,** 78 (2016).

[8] J. Hafner, S. Benaglia, F. Richheimer, M. Teuschel, F. J. Maier, A. Werner, S. Wood, D. Platz, M. Schneider, K. Hradil, F. A. Castro, R. Garcia, and U. Schmid, Multiscale characterisation of a ferroelectric polymer reveals the emergence of a morphological phase transition driven by temperature, Nat. Commun. **12,** 152 (2021).

[9] T. Furukawa and N. Seo, Electrostriction as the origin of piezoelectricity in ferroelectric polymers, Jpn. J. Appl. Phys. **29,** 675 (1990).

[10] Y. Liu, H. Aziguli, B. Zhang, W. Xu, W. Lu, J. Bernholc, and Q. Wang, Ferroelectric polymers exhibiting behaviour reminiscent of a morphotropic phase boundary, Nature **562,** 96 (2018).

[11] P. Hu, S. Hu, Y. Huang, J. R. Reimers, A. M. Rappe, Y. Li, A. Stroppa, and W. Ren, Bioferroelectric properties of glycine crystals, J. Phys. Chem. Lett. **10,** 1319 (2019).

[12] V. S. Bystrov, E. Seyedhosseini, I. Bdikin, S. Kopyl, S. M. Neumayer, J. Coutinho, and A. L. Kholkin, Bioferroelectricity in nanostructured glycine and thymine: Molecular modeling and ferroelectric properties at the nanoscale, Ferroelectrics **475,** 107 (2015).

[13] Z. Zhang, X. Li, Z. Peng, X. Yan, S. Liu, Y. Hong, Y. Shan, X. Xu, L. Jin, B. Liu, X. Zhang, Y. Chai, S. Zhang, A. K. Y. Jen, and Z. Yang, Active self-assembly of piezoelectric biomolecular films via synergistic nanoconfinement and insitu poling, Nat. Commun. **14,** 4094 (2023).

[14] F. Lv, J. Lin, Z. Zhou, Z. Hong, Y. Wu, Z. Ren, Q. Zhang, S. Dong, J. Luo, J. Shi, R. Chen, B. Liu, Y. Su, and Y. Huang, *In-situ* electrostatic field regulating the recrystallization behavior of P(VDF-TrFE) films with high β-phase content and enhanced piezoelectric properties towards flexible wireless biosensing device applications, Nano Energy **100,** 107507 (2022).

[15] R. W. Greaves and D. R. Lamb, Observation of the inverse piezoelectric effect in polyethylene while under a polarising field, J. Mater. Sci. **6,** 74 (1971).

[16] R. L. Zimmerman, C. Suchicital, and E. Fukada, Electric field-induced piezoelectricity in polymer film, J. Appl. Polym. Sci. **19,** 1373 (1975).

[17] M. M. Yang, Z. D. Luo, Z. Mi, J. Zhao, E. Sharel Pei, and M. Alexe, Piezoelectric and pyroelectric effects induced by interface polar symmetry, Nature **584,** 377 (2020).

[18] O. Aktas, M. Kangama, G. Linyu, G. Catalan, X. Ding, A. Zunger, and E. K. H. Salje, Piezoelectricity in nominally centrosymmetric phases, Phys. Rev. Res. **3,** 043221 (2021).

[19] E. J. Murphy and S. O. Morgan, The dielectric properties of insulating materials, Bell Syst. Tech. J. **16,** 493 (1937).

[20] X. Chen, H. Qin, X. Qian, W. Zhu, B. Li, B. Zhang, W. Lu, R. Li, S. Zhang, L. Zhu, F. D. D. Santos, J. Bernholc, and Q. M. Zhang, Relaxor ferroelectric polymer exhibits ultrahigh electromechanical coupling at low electric field, Science **375,** 1418 (2022).

[21] See the Supplemental Material at http://link.aps.org/supplemental/10.1103/PhysRevApplied.22.014077 for supplementary Figs. S1–S23; it also includes Refs. [24,39–41].

[22] W. Li, Q. Meng, Y. Zheng, Z. Zhang, W. Xia, and Z. Xu, Electric energy storage properties of poly(vinylidene fluoride), Appl. Phys. Lett. **96,** 192905 (2010).

[23] R. E. Cohen, Origin of ferroelectricity in perovskite oxides, Nature **358,** 136 (1992).

[24] O. R. Hughes, Frequency dependence of hysteresis associated with the electromechanical performance of PVDF film, J. Polym. Sci., Part B: Polym. Phys. **45,** 3207 (2007).

[25] J. C. Hicks and T. E. Jones, Frequency dependence of remanent polarization and the correlation of piezoelectric coefficients with remanent polarization in polyvinylidene fluoride, Ferroelectrics **32,** 119 (1981).

[26] D. Damjanovic, A morphotropic phase boundary system based on polarization rotation and polarization extension, Appl. Phys. Lett. **97,** 062906 (2010).

[27] K. Uchino, S. Nomura, L. E. Cross, R. E. Newnham, and S. J. Jang, Electrostrictive effect in perovskites and its transducer applications, J. Mater. Sci. **16,** 569 (1981).

[28] D.-S. Park, M. Hadad, L. M. Riemer, R. Ignatans, D. Spirito, V. Esposito, V. Tileli, N. Gauquelin, D. Chezganov, D. Jannis, J. Verbeeck, S. Gorfman, N. Pryds, P. Muralt, and D. Damjanovic, Induced giant piezoelectricity in centrosymmetric oxides, Science **375,** 653 (2022).

[29] H. Zhang, N. Pryds, D.-S. Park, N. Gauquelin, S. Santucci, D. V. Christensen, D. Jannis, D. Chezganov, D. A. Rata, A. R. Insinga, I. E. Castelli, J. Verbeeck, I. Lubomirsky, P. Muralt, D. Damjanovic, and V. Esposito, Atomically engineered interfaces yield extraordinary electrostriction, Nature **609,** 695 (2022).

[30] R. E. Newnham, V. Sundar, R. Yimnirun, J. Su, and Q. M. Zhang, Electrostriction: Nonlinear electromechanical coupling in solid dielectrics, J. Phys. Chem. B **101,** 10141 (1997).

[31] F. Li, Breaking symmetry for piezoelectricity, Science **375,** 618 (2022).

[32] J. Kuwata, K. Uchino, and S. Nomura, Electrostrictive coefficients of $Pb(Mg_{1/3}Nb_{2/3})O_3$ ceramics, Jpn. J. Appl. Phys. **19,** 2099 (1980).

[33] P. Xiao, N. Yi, T. Zhang, Y. Huang, H. Chang, Y. Yang, Y. Zhou, and Y. Chen, Construction of a fish-like robot based on high performance graphene/PVDF bimorph actuation materials, Adv. Sci. **3,** 1500438 (2016).

[34] M. J. Haun, E. Furman, S. J. Jang, and L. E. Cross, Thermodynamic theory of the lead zirconate-titanate solid-solution system, part 1: Phenomenology, Ferroelectrics **99,** 13 (1989).

[35] M. E. Lines and A. M. Glass, *Principles and Applications of Ferroelectrics and Related Materials* (Oxford University Press, Oxford, 1977).

[36] M.-H. Zhang, *et al.*, Deciphering the phase transition-induced ultrahigh piezoresponse in $(K, Na)NbO_3$-based piezoceramics, Nat. Commun. **13,** 3434 (2022).

[37] M. Aslam, M. A. Kalyar, and Z. A. Raza, Polyvinyl alcohol: A review of research status and use of polyvinyl alcohol based nanocomposites, Polym. Eng. Sci. **58,** 2119 (2018).

[38] S. J. L. Billinge, The rise of the x-ray atomic pair distribution function method: A series of fortunate events, Philos. Trans. R. Soc., A **377,** 20180413 (2019).

[39] R. K. Tubbs, Melting point and heat of fusion of poly(vinyl alcohol), J. Polym. Sci., Part A: Polym. Chem. **3,** 4181 (1965).

[40] F. Reguieg, L. Ricci, N. Bouyacoub, M. Belbachir, and M. Bertoldo, Thermal characterization by DSC and TGA analyses of PVA hydrogels with organic and sodium MMT, Polym. Bull. **77,** 929 (2020).

[41] N. A. Peppas and P. J. Hansen, Crystallization kinetics of poly(vinyl alcohol), J. Appl. Polym. Sci. **27,** 4787 (1982).

[42] J. Mavračić, F. C. Mocanu, V. L. Deringer, G. Csányi, and S. R. Elliott, Similarity between amorphous and crystalline phases: The case of TiO_2, J. Phys. Chem. Lett. **9,** 2985 (2018).

[43] M. Ponçot, F. Addiego, and A. Dahoun, True intrinsic mechanical behaviour of semi-crystalline and amorphous polymers: Influences of volume deformation and cavities shape, Int. J. Plast. **40,** 126 (2013).

[44] L. You, Y. Zhang, S. Zhou, A. Chaturvedi, S. A. Morris, F. Liu, L. Chang, D. Ichinose, H. Funakubo, W. Hu, T. Wu, Z. Liu, S. Dong, and J. Wang, Origin of giant negative piezoelectricity in a layered van der Waals ferroelectric, Sci. Adv. **5,** eaav3780 (2019).

[45] A. Heredia, V. Meunier, I. K. Bdikin, J. Gracio, N. Balke, S. Jesse, A. Tselev, P. K. Agarwal, B. G. Sumpter, S. V. Kalinin, and A. L. Kholkin, Nanoscale ferroelectricity in crystalline γ-glycine, Adv. Funct. Mater. **22,** 2996 (2012).

[46] B. Wu, C. Mu, G. Zhang, and W. Lin, Effects of Cr3+ on the structure of collagen fiber, Langmuir **25,** 11905 (2009).

[47] Z. Zhang, S. Liu, Q. Pan, Y. Hong, Y. Shan, Z. Peng, X. Xu, B. Liu, Y. Chai, and Z. Yang, van der Waals exfoliation processed biopiezoelectric submucosa ultrathin films, Adv. Mater. **34,** 2200864 (2022).

[48] X. Kuang, Q. Gao, and H. Zhu, Effect of calcination temperature of TiO_2 on the crystallinity and the permittivity of PVDF-TrFE/TiO_2 composites, J. Appl. Polym. Sci. **129,** 296 (2013).

[49] D. Singh, N. L. Singh, P. Kulriya, A. Tripathi, and D. M. Phase, ac electrical and structural properties of polymethylmethacrylate/aluminum composites, J. Compos. Mater. **44,** 3165 (2010).